International Conference on Space Optics—ICSO 2020

Virtual Conference

30 March–2 April 2021

Edited by Bruno Cugny, Zoran Sodnik, and Nikos Karafolas

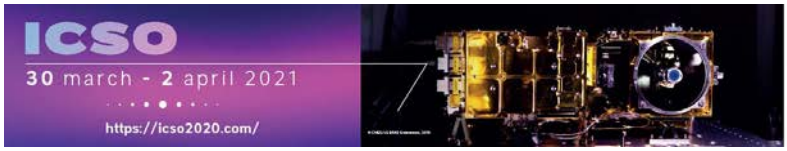

Performance analysis of polar-code transmission experiments over 7.8-km terrestrial free-space optical link using channel equalization

International Conference on Space Optics — ICSO 2020, edited by Bruno Cugny, Zoran Sodnik, Nikos Karafolas, Proc. of SPIE Vol. 11852, 118525K · © 2021 ESA and CNES
CCC code: 0277-786X/21/$21 · doi: 10.1117/12.2599963

Performance analysis of polar-code transmission experiments over 7.8-km terrestrial free-space optical link using channel equalization

S. Fujita[a] E. Okamoto[a] H. Takenaka[b] H. Kunimori[b] H. Endo[b] M. Fujiwara[b]
M. Kitamura[b] R. Shimizu[c] M. Sasaki[b] and M. Toyoshima[b]

[a]Department of Electrical and Mechanical Engineering, Graduate School of Engineering, Nagoya Institute of Technology Gokiso-cho, Showa-ku, Nagoya, Aichi 466-8555, Japan.
[b]National Institute of Information and Communications Technology
Nukui-Kitamachi 4-2-1, Koganei, Tokyo 184-0014 Japan.
[c]Faculty of Informatics and Engineering, University of Electro-Communications
Chofugaoka 1-5-1, Chofu, Tokyo 182-8585, Japan.

ABSTRACT

Satellite laser communication is a promising solution to satisfy the increasing demand for high-capacity wireless communications. Satellite laser communication has several advantages over its radio frequency counterparts, such as a higher capacity with a broader bandwidth and transmission security provided by highly directional laser beams. However, the received optical power fluctuations induced by atmospheric scintillation cause burst errors, requiring the employment of high-performance error correction codes, such as turbo or low-density parity check (LDPC) codes. Recently, polar code has been attracting significant attention, primarily because of its lower encoding and decoding computational complexity and its high performance, reaching the Shannon limit. We have reported a long-distance experiment using 7.8-km terrestrial free-space optical (FSO) communication links and compared the performance of polar and LDPC codes. Our experimental results revealed the advantage of polar codes over LDPC codes when channel state information (CSI) was not available. In FSO communications suffering from atmospheric fading, it is known that we can enhance the error-correction performance of these codes by utilizing a channel equalization technique based on the estimated CSI. In this study, we present the results of long-distance transmission experiments using polar codes with channel equalization. As a result, equalization improves the error-correction performance. Moreover, even with channel equalization, the block error rate of polar codes is better than that of LDPC codes, as in our previous report.

Keywords: free space optics, transmission experiments, polar code, low-density parity check code, channel equalization

1. INTRODUCTION

In recent years, the demand for high-capacity wireless communication has continually increased. In particular, as Internet of things (IoT) and artificial intelligence (AI) become more widespread, the data capacity and the number of communication terminals are expected to increase. Against this background, the use of satellites as well as terrestrial networks are considered a solution to these problems [1]. In particular, optical satellite communication is expected to be the next generation space communication method because it can provide higher capacity communication than radio-wave satellite communication. The National Institute of Information and Communications Technology (NICT) and other organizations have been researching practical application of optical satellite communications [2]. Optical satellite communication can not only be the high capacity transmission but also ensure communication confidentiality and less interference with the strong laser beam directivity [3]. However, owing to the strong directivity, high-precision directional technology is required to accurately capture the transmission. In addition, atmospheric turbulence between the ground and satellite causes degradation of the received power, which degrades communication quality. Then, the powerful forward error correction (FEC), such as low-density parity check (LDPC) codes [4] and turbo codes [5] are required, and many FEC studies on these and other codes for satellite laser communication have been conducted.

Conversely, polar codes, a strong linear channel code, have been recently proposed by [6]. It has been rigorously proven that polar codes can be implemented with a computational complexity of $O(N\log N)$ for coding and decoding of N [bits]

code length, and can asymptotically achieve a communication channel's capacity at long code lengths. It is also known that polar codes concatenated with cyclic redundancy check (CRC) codes can be decoded by successive cancellation list decoding (SCLD) and have improved performance over LDPC codes with a short code length [7]. Owing to this excellent performance, they are used as error-correcting codes for control channels in the 5th generation (5G) mobile communications system.

We have studied the application of polar codes to spatial optical communication by numerical simulations and demonstrated that they can provide excellent performance [8]. Subsequently, we conducted a field experiment of polar codes in a 7.8-km optical spatial communication testbed between the University of Electro-Communications and NICT, and analyzed the transmission performance in a practical environment [9]. The results show that polar codes have superior performance compared to LDPC codes in the absence of channel information. However, the decoding performance of LDPC and polar codes is degraded by the deterioration of the log-likelihood ratio (LLR) in the absence of channel state information (CSI).

Therefore, in this study, we propose a method to improve the decoding performance of polar codes by channel estimation and equalization based on transmission experiments in long-distance terrestrial free-space optical (FSO) communication, and demonstrate its superior performance.

The remainder of this paper is organized as follows: Section 2 provides a brief review of polar encoding and decoding. Section 3 details the atmospheric fluctuation model, which is typical for optical satellite communications. Section 4 outlines the transmission experiments, and Section 5 presents the experimental results and compares them with the simulation results. Finally, Section 6 concludes the paper.

2. POLAR CODES

2.1 Encoding

The vector consisting of $(a_0, \cdots, a_{N-1})$ is denoted as $\boldsymbol{a}_0^{N-1}$. The channel conditional probability is denoted as $W(y|x)$, where the input $x \in X = \{0,1\}$ and output $y \in Y$, $\mathrm{Y} \in \mathbb{R}$. Consider the case where the code length $N = 2^n$ and $n \geq 0$, and Figure 1 shows the encoder construction with $N = 8$. The generator matrix $\mathbf{G}_N$ for code length N is recursively calculated as follows:

$$\begin{aligned} \mathbf{G}_N &= \mathbf{R}_N(\mathbf{F}\otimes\mathbf{I}_{N/2})(\mathbf{I}_2\otimes\mathbf{G}_{N/2}) \\ \mathbf{G}_1 &= \mathbf{I}_1, \end{aligned} \tag{1}$$

where $\mathbf{I}_N$ is a unit matrix of order N, and $\otimes$ is the Kronecker product. $\mathbf{R}_N$ is a reverse shuffle matrix that reorders the vectors into even and odd indices, defined by,

$$\mathbf{x}_0^{N-1}\mathbf{R}_N = (x_0,\ x_2,\ \cdots,\ x_{N-2},\ x_1,\ x_3,\ \cdots,\ x_{N-1}). \tag{2}$$

The matrix **F** is defined by,

$$\mathbf{F} = \begin{bmatrix} 1 & 0 \\ 1 & 1 \end{bmatrix}. \tag{3}$$

The codewords $\mathbf{x}_0^{N-1}$ for the information word $\mathbf{u}_0^{N-1}$can be obtained by,

$$\mathbf{x}_0^{N-1} = \mathbf{u}_0^{N-1}\mathbf{G}_N. \tag{4}$$

The effect of polar encoding on $\mathbf{u}_0^{N-1}$ consists of a recursive iteration of the channel duplication and combination. The channel capacity is asymptotically divided into a set F of zeroes and a set $\bar{F}$ of ones. When the information bit length is infinite, the capacity converges to "0" or "1". Here, by fixing the input value to zero as the frozen bit for the bits with a communication channel capacity of zero, the information bits can be transmitted without error for the bits with a communication channel capacity of one.

2.2 Successive cancellation decoding

Polar codes are generally decoded by successive cancellation decoding (SCD) [6]. In SCD, each bit is decoded based on the LLR in ascending order of index i. The $L_N^{(i)}$ is the LLR, which is defined by,

$$L_N^{(i)} \triangleq \ln\frac{W\left(\mathbf{y}_0^{N-1},\mathbf{u}_0^{i-1}|0\right)}{W\left(\mathbf{y}_0^{N-1},\mathbf{u}_0^{i-1}|1\right)}. \tag{5}$$

In on-off keying (OOK), the initial value of the LLR is defined as,

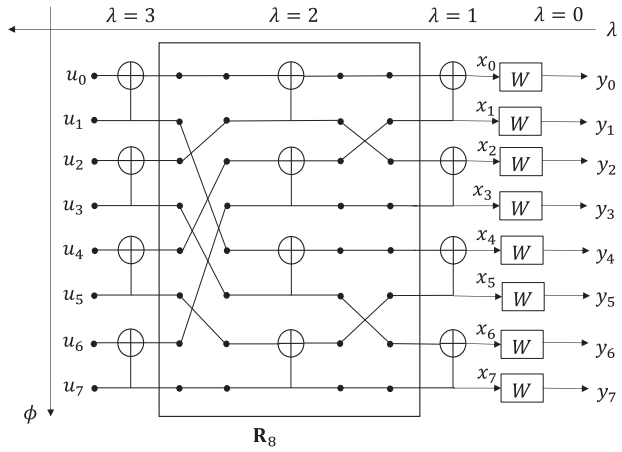

Figure 1. Construction of encoder $\mathbf{G}_8$

$$L_0^{(i)} = \frac{h_i^2 - 2h_i y_i}{2\sigma^2}, \tag{1}$$

where σ^2 is the noise variance, and h_i is the fading coefficient for the i-th bit. In SCD, the LLR is recursively calculated by,

$$L_\lambda^{(2\phi)} = f\left(L_{\lambda-1}^{(2\phi-[\phi \bmod 2^{\lambda-1}])}, L_{\lambda-1}^{(2^\lambda+2\phi-[\phi \bmod 2^{\lambda-1}])}\right), \tag{2}$$

$$L_\lambda^{(2\phi+1)} = g\left(L_{\lambda-1}^{(2\phi-[\phi \bmod 2^{\lambda-1}])}, L_{\lambda-1}^{(2^\lambda+2\phi-[\phi \bmod 2^{\lambda-1}])}, u_{0,e}^{2i} \oplus u_{0,o}^{2i}\right), \tag{3}$$

where ϕ and λ are defined as $0 \le \phi \le N/2$ and $0 \le \lambda \le n$, respectively. ϕ corresponds to the vertical index of the encoder, and λ corresponds to the horizontal index, as shown in Figure 1. In addition, $u_{0,e}^{2i}$, and $u_{0,o}^{2i}$ refer to the even and odd elements in u_0^{2i}, respectively. The output f and g functions are defined as follows:

$$f(L_\alpha, L_\beta) = 2\tanh^{-1}\left(\tanh\left(\frac{L_\alpha}{2}\right)\tanh\left(\frac{L_\beta}{2}\right)\right), \tag{4}$$

$$g(L_\alpha, L_\beta, \hat{u}) = L_\alpha + (-1)^{\hat{u}} L_\beta, \tag{10}$$

where L_α and L_β are the decoder LLR inputs and $\hat{u}$ is obtained by the estimation bit. This calculation is repeated until the $L_N^{(i)}$ is obtained. The i-th estimation bit $\hat{u}_i$ is obtained as follows:

$$\hat{u}_i \triangleq \begin{cases} u_i, & i \in F \\ 0, & i \in \bar{F}, \text{and } L_N^{(i)} \ge 0. \\ 1, & i \in \bar{F}, \text{and } L_N^{(i)} < 0 \end{cases} \tag{11}$$

The use of SCLD has also been proposed as a decoding algorithm to improve the SCD properties. The SCLD stores the sequences of L_{max} highest likelihood, that is, small path metric in the SCD process, and finally, the highest likelihood sequence of the list among L_{max} candidate sequences is selected as the decoding result [10]. The path metric at the l-th path and i-th bit is defined by,

$$PM_l^{(i)} \triangleq \sum_{j=0}^{i} \ln\left(1 + \mathrm{e}^{-(1-2\,\hat{u}_j[l])L_n^{(j)}[l]}\right), \tag{12}$$

where $\hat{u}_j[l]$ and $L_n^{(j)}[l]$ are the values of the decoding bit $\hat{u}_j$ and LLR L_n^j in the l-th pass, respectively. Decoding with SCLD increases the decoding complexity to $O(L_{max}N\log N)$ but provides better performance than SCD.

2.3 CRC-aided successive cancellation decoding

The CRC-aided successive cancellation decoding (CA-SCLD) has been proposed to further improve polar code performance [7]. The CRC codes are widely used in wireless communication systems. k CRC bits are added to $K - k$

information bits at the transmitter side, and K is the information length input to the polar encoder. For each of these K bits, the $N-K$ frozen bits are set and encoded. At the receiver side, the data are decoded by SCLD, and error detection is performed by the CRC codes for each of the resulting L_{max} candidate sequences. The sequence that detected no error by the CRC check was recognized as the decoding result. Therefore, the performance can be significantly improved compared with SCLD, and it provides better performance than LDPC codes with a short code length.

3. ATMOSPHERIC PROPAGATION MODEL IN FADING CHANNEL

In FSO channels, the optical intensity fluctuates owing to atmospheric turbulence at the receiver side. The gamma-gamma distribution is known as the distribution function that expresses the intensity fluctuation [11]. The probability density function (PDF) of intensity I of a gamma-gamma distribution is given by,

$$p_I(I;\alpha,\beta) = \frac{2(\alpha\beta)^{\frac{\alpha+\beta}{2}}}{\Gamma(\alpha)\Gamma(\beta)} I^{\frac{\alpha+\beta}{2}-1} K_{\alpha-\beta}(2\sqrt{\alpha\beta I}), \tag{13}$$

where $K_n(z)$ is the modified Bessel function of the second type of order n, and $\Gamma()$ is the gamma function. α and β are the independent stochastic parameters of the small- and large-scale scintillation indexes, given by,

$$\alpha = \left(\exp\left[\frac{0.49\sigma_R^2}{\left(1+1.11\sigma_R^{\frac{12}{5}}\right)^{\frac{7}{6}}} \right] - 1 \right)^{-1}. \tag{14}$$

$$\beta = \left(\exp\left[\frac{0.51\sigma_R^2}{\left(1+0.69\sigma_R^{\frac{12}{5}}\right)^{\frac{7}{6}}} \right] - 1 \right)^{-1}, \tag{15}$$

where σ_R^2 is the scintillation index (SI), used as a degree of atmospheric fluctuation index. In the gamma-gamma distribution, SI is given by,

$$\sigma_R^2 = \frac{\langle I^2 \rangle}{\langle I \rangle^2} - 1. \tag{16}$$

Eq. (16) shows that when SI is small, the variation is small, and when SI is large, the variation is larger than the average value.

4. OUTLINE OF EXPERIMENTS

We confirmed the performance of polar codes in an actual environment by conducting transmission experiments using an optical communication testbed between the University of Electro-Communications and NICT [9]. It is necessary to use CSI to obtain the correct LLR in a channel with fluctuating optical intensity. We describe the experimental outline using channel estimation and equalization for performance improvement.

The transmission experiment was performed using an optical communication testbed [12–14] with a linear distance of approximately 7.8 km, as shown in Figure 2, which consists of a transmission system in an all-weather dome-shaped facility on a building at the University of Electro-Communications site and a detection system on the sixth floor of a building at the NICT site. In this experiment, the Lena image shown in Figure 3 was encoded and transmitted. Figure 4 shows a block diagram of the transmitter. A continuous wave (CW) laser with a central wavelength of 1550 nm was used as the transmitter side light source. The signal was generated by inputting the pre-prepared codeword and pilot symbols into an arbitrary waveform generator (AWG) and transmitted by on-off keying with a bandwidth of 10 Mbps. The optical signal is amplified and coupled from a single-mode fiber (SMF) to a fiber collimator, and then expanded to an approximately 5.5 mm diameter beam for transmission.

Figure 5 shows a block diagram of the receiver. At the receiver, the optical signal was collected by the Cassegrain telescope on the 6th floor and then coupled to the multi-mode fiber (MMF). Optical intensity was detected using a photodiode (PD). The detector signal was amplified and band-limited to 20 MHz using a low-pass filter (LPF), and then measured using an oscilloscope (sampling rate: 50 MHz). The data were inputted offline to the decoder. The received pilots were used for the channel estimation and equalization.

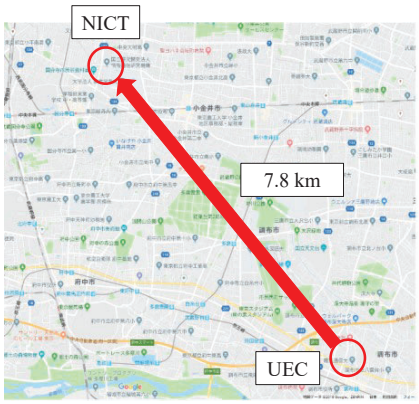

Figure 2. Location of the experimental system (©2020 Google).

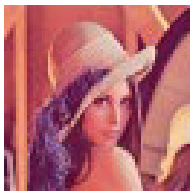

Figure 3. Transmitted Lena image

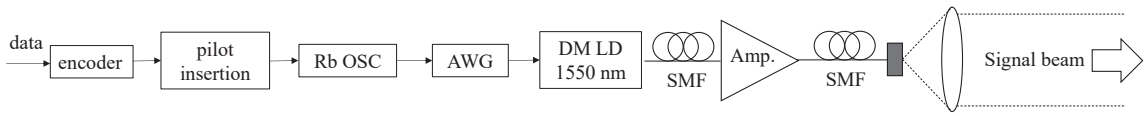

Figure 4. Block diagram of the transmitter.

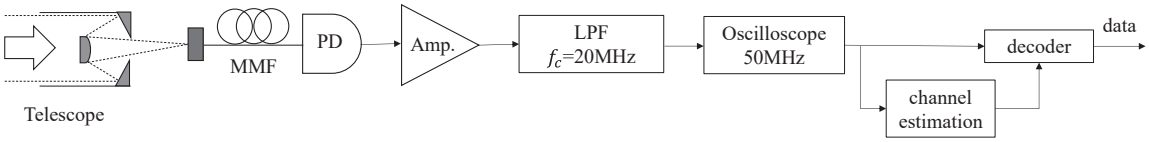

Figure 5. Block diagram of the receiver.

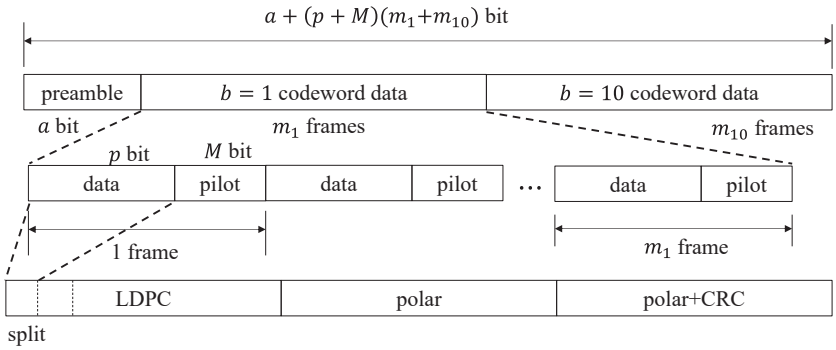

Figure 6. Transmission data format.

Figure 6 and Table 1 show the transmission data format for this experiment and the experimental conditions, respectively. The Lena image was encoded by LDPC and polar codes with a CRC code of $k = 24$ bits, and two block types interleaving with depth $b = 1, 10$ bits were applied to each. The code length was $N = 2048$ bits, the code rate was 0.5, and when the number of information bits was less than $K = 1024$ bits, it was padded with a continuous pattern of "01." In addition, a preamble was inserted for synchronization. To perform channel estimation, pilot symbols were inserted for every p-bit of the codewords. The pilot symbol is a sequence of M bits with an iterative 01 pattern, and CSI is the average of the received values when "1" is transmitted. In one transmission sequence, there were m_1 frames of $(p + M)$ bits for $b = 1$, and m_{10} frames for $b = 10$. Therefore, the total number of bits is $a + (p + M)(m_1 + m_{10})$ bits. In this experiment, a pilot symbol of $M = 128$ bits was inserted for every $p = 512$ bits of codewords. The channel variation was assumed to be constant and fixed during this 512-bit period. The preamble is inserted at $a = 256$ bits.

TABLE I. EXPERIMENTAL CONDITIONS.

Code	*Polar*	*LDPC*
Code length	2048	
Code rate	0.5	
Modulation	on-off keying	
Column and row weights	N/A	(6,3)
CRC length	24	N/A
Decoding algorithm	SCLD	Sum-product decoding
List size	32	N/A
Number of decoding iterations	N/A	50
Bit rate	10 Mbps	
Block interleaver depth b	1, 10	
Experimental date and time	January 29, 2020 18:00 – January 31, 2020 13:00	

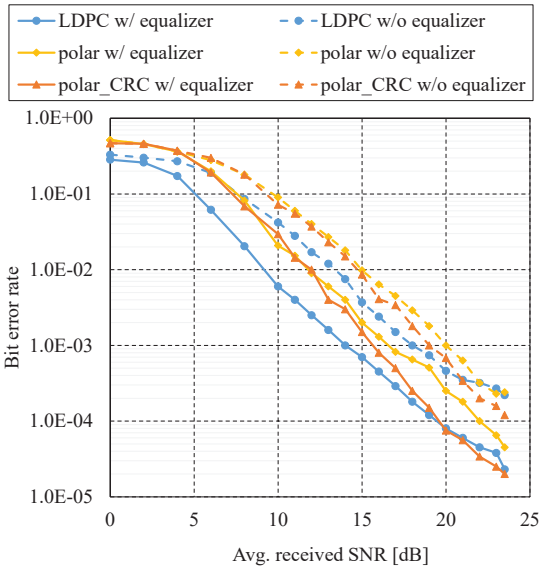

Figure 7. Experimental results of BER performance.

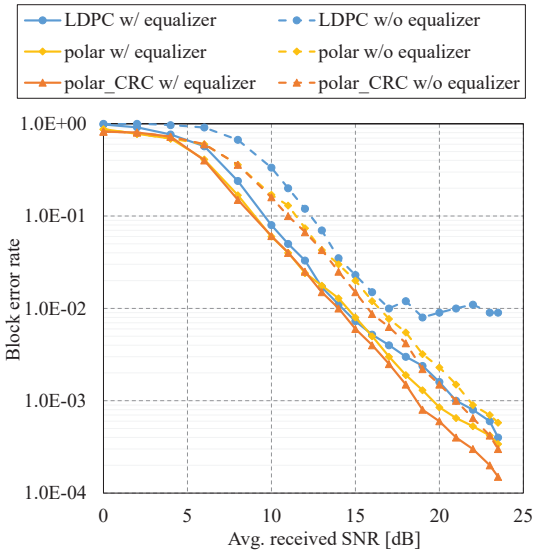

Figure 8. Experimental results of BLER performance.

5. EXPERIMENTAL RESULTS

5.1 Transmission performance

Figures 7 and 8 show the bit error rate (BER) and block error rate (BLER) performance, respectively, where the horizontal axis is the average signal-to-noise ratio (SNR) at the receiver side. The legend *w/equalizer* indicates that channel equalization is performed using CSI. Because the OOK decoding performance is significantly degraded when CSI is not available and directly demodulated, the demodulation in which the received voltage is shifted and 1/2-amplitude BPSK demodulation is equivalently used to suppress the degradation.

The results show that the performance of both polar and LDPC codes is improved by using CSI. In particular, the error floor of the BLER in LDPC codes is improved by equalization. This is because the use of CSI improves the quality of the LLR and enhances decoding performance. In addition, the LDPC code shows better BER performance, whereas the BLER performance with polar codes is better. This is because polar codes are sequentially decoded, and if one bit is misdecoded, the error is propagated, resulting in more bit errors per codeword. In addition, the channel equalization effect is emphasized more for LDPC codes because polar codes are less sensitive to LLR degradation. The reason is as follows: For simplicity, we consider the case of an all zero codeword. In polar codes, if $\hat{u}_i$ can be correctly decoded, the output LLR becomes large because the two LLRs are added in Eq. (10). In other words, if the decoding to that point can be correctly performed, the decoding can proceed by increasing the LLR. Therefore, even if the LLR is degraded, the negative effect on the decoding

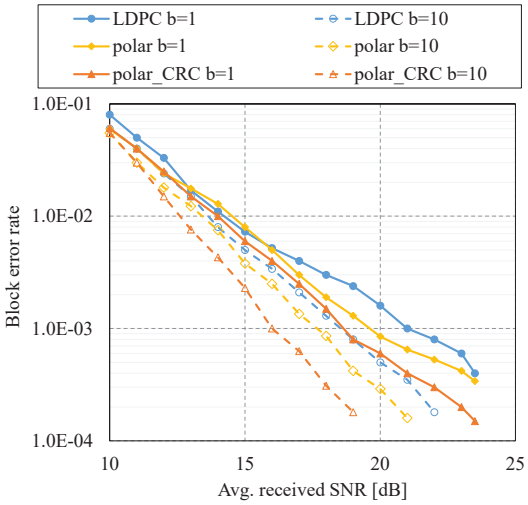

Figure 9. BLER performance applied to block interleaving.

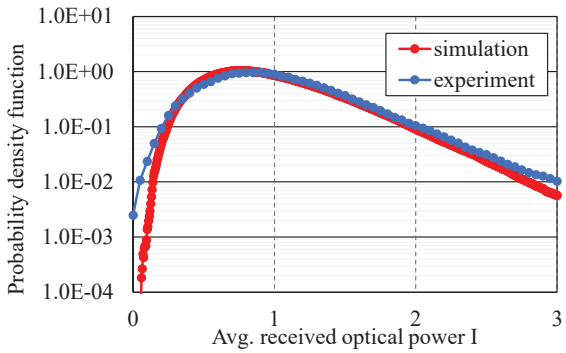

Figure 10. PDF of the intensity variation.

TABLE II. SIMULATION CONDITIONS

Code	***Polar***	***LDPC***
Code length	2048	
Code rate	0.5	
Modulation	on-off keying	
Column and row weight	N/A	(6,3)
CRC length	24	N/A
Decoding algorithm	SCLD	Sum-product decoding
List size	32	N/A
Number of decoding iterations	N/A	50
Channel model	Atmospheric fluctuation with AWG	
Intensity fluctuation probability distribution	gamma-gamma distribution	
SI	0.2	
Sampling time Δt	1.0×10^{-7} sec	
Block interleaver depth b	10	

process is less than that of the LDPC codes. Thus, even when LDPC codes cannot fully correct errors owing to the LLR degradation, polar codes can be decoded without a BLER error floor. The BER performance of polar codes with CRC codes is better than those of LDPC codes in the high SNR region. This is because in the high SNR region, the correct sequences are easily included, and the error detection by the CRC code can select the correct sequences.

Figure 9 shows the BLER performance with block interleaving when using channel equalization. From the results, it can be seen that block interleaving improves the performance because the interleaver spreads burst errors and improves LLR quality in the decoding process. Furthermore, when comparing the three codes, it is obvious that the polar code with CRC and interleaving has the best performance.

5.2 Comparison with numerical results

First, we calculated the average SI over the experimental period using Eq. (16) for the received data, and the result is SI $\fallingdotseq$ 0.2. Figure 10 shows the PDF of the intensity variation in the experiment and the simulation result for SI = 0.2. The results show that the general shapes are approximately the same. Although there are some deviations, the intensity fluctuation model for FSO communication can be expressed using the gamma-gamma distribution. As seen, there are deviations from the simulation near both ends of the horizontal axis. This is probably owing to the intensity fluctuation

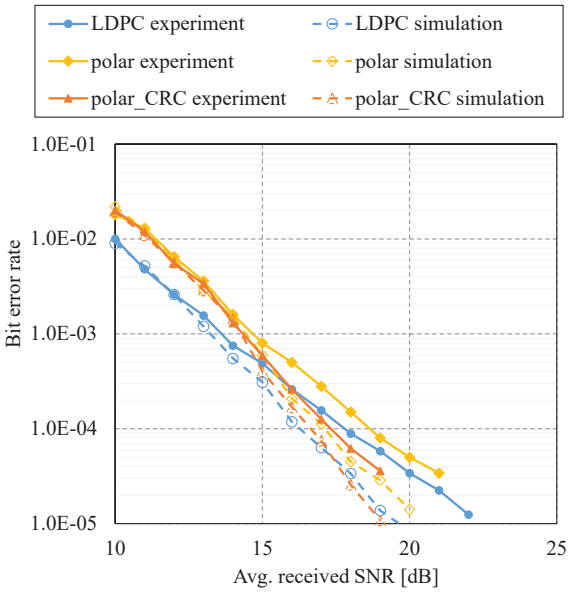

Figure 11. BER comparison of experiment and simulation results.

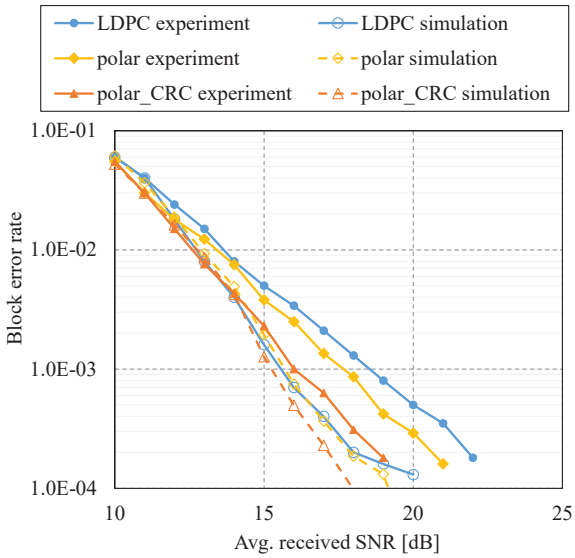

Figure 12. BLER comparison of experiment and simulation results.

model difference in the actual environment and the noise generated in the experimental system. Next, we compared the simulation and experimental results of the polar and LDPC codes using the calculated SI, where the simulation conditions are shown in Table 2, and the BER and BLER performance results are shown in Figures 11 and 12, respectively.

The channel was assumed to be a time-correlated gamma-gamma distribution. In this simulation, the channel is estimated every 512 bits, as in the experiment, and the channel variation is assumed to be constant during the estimation. The simulation results show that the LDPC codes are better in terms of BER performance and polar codes in terms of BLER performance. This is because, as explained in Section 5.1, the BER performance of polar codes tends to become increasingly worse when decoding fails. Additionally, in the high SNR region, the difference between the experimental and simulation results is large, which is thought to be caused by the intensity fluctuation model difference between the actual and simulated environments and the effect of non-white noise in the experimental environment. These results show that polar codes are more effective than LDPC codes, especially in terms of BLER performance. In addition, we confirmed that the performance of polar codes can be further improved by connecting CRC codes.

6. CONCLUSION

In this study, we evaluated the performance of error correcting codes with channel estimation and equalization of polar-coded terrestrial FSO transmission experiments over a long distance of 7.8 km. From the results, the decoding performance of the codes can be improved by channel equalization. Moreover, even with channel equalization, the BLER of polar codes is better than that of LDPC codes.

REFERENCES

[1] Evans, B. G., “The role of satellites in 5G,” IEEE 7th ASMS Conference, 197–202, (2014).
[2] Arai, K., “Overview of the Optical Inter-orbit Communications Engineering Test Satellite (OICETS) Project,” Special issue of J NICT, 2, 59(1,2), (2012).
[3] Toyoshima, M., Kuri, T., Werner, K., Toyoda, M., Takenaka, H., Shoji, Y., Takayama, Y., Koyama, Y., Kunimori, H., Jono, K., Yamakawa, S., and Arai, K., “Overview of the Laser Communication System for the NICT Optical Ground Station and Laser Communication Experiments on Ground-to-Satellite Links,” J. Nat. Inst. Inf. and

Commun. Tech., 59(1,2), 53–75, (2012).

[4] Gallager, R. G., “Low-Density Parity-Check Codes,” IRE Trans. Inf. Theory, 8(1), 21–28, (1962).

[5] Berrou, C., et.al, “Near Shannon limit error-correcting coding and decoding: Turbo-codes,” in Proc. IEEE Int. Conf. on Commun. 93, (1993).

[6] Arıkan, E., “Channel polarization: A method for constructing capacity-achieving codes for symmetric binary-input memoryless channels,” IEEE Trans. Inf. Theory, 55(7), 3051–3073, (2009).

[7] Niu K. and Chen, K., “CRC-Aided Decoding of Polar Codes,” IEEE Commun. Lett., 16(10), 1668–1671, (2012).

[8] Ito, K., Okamoto, E., Takenaka, H., Kunimori, H., and Toyoshima, M., “An adaptive coded transmission scheme utilizing frozen bits of polar code in satellite laser communications,” Proc. ICSO, 1–7, (2018).

[9] Fujita, S., Ito, K., Okamoto, E., Takenaka, H., Kunimori, H., Endo, H., Fujiwara, M., Kitamura, M., Shimizu, R., Sasaki, M., and Toyoshima M., “Experimental evaluation of polar code transmission in terrestrial free space optics,” Proc. IEEE ICSOS, 1–6, (2019).

[10] Tal I. and Vardy, A., “List decoding of polar codes,” IEEE Trans. Inf. Theory, 61(5), 2213–2226, (2011).

[11] Bykhovsky, D., “Simple generation of Gamma, Gamma-Gamma, and K distributions with exponential autocorrelation function,” IEEE J Light. Technol., 34(9), 2106–2110, (2016).

[12] Endo, H., Fujiwara, M., Kitamura, M., Ito, T., Toyoshima, M., Takayama, Y., Takenaka, H., Shimizu, R., Laurenti, N., Vallone, G., Villoresi, P., Aoki, T., and Sasaki, M., "Free-space optical channel estimation for physical layer security," Opt. Express, 24(18), 8940–8955, (2016).

[13] Fujiwara, M., Ito, T., Kitamura, M., Endo, H., Tsuzuki, O., Toyoshima, M., Takenaka, H., Takayama, Y., Shimizu, R., Takeoka, M., Matsumoto, R., and Sasaki, M., “Free-space optical wiretap channel and experimental secret key agreement in 7.8 km terrestrial link,” Opt. Express, 26(15), 19513–19523, (2018).

[14] Endo, H., Fujiwara, M., Kitamura, M., Tsuzuki, O., Ito, T., Shimizu, R., Takeoka, M., and Sasaki, M., “Free space optical secret key agreement,” Opt. Express, 26(18), 23305–23332, (2018).